ACS APPLIED MATERIALS & INTERFACES

Research Article

www.acsami.org

Composite Polymer Electrolytes with $Li_7La_3Zr_2O_{12}$ Garnet-Type Nanowires as Ceramic Fillers: Mechanism of Conductivity Enhancement and Role of Doping and Morphology

Ting Yang,[†] Jin Zheng,[‡] Qian Cheng,[†] Yan-Yan Hu,[‡,§] and Candace K. Chan*[,†]

[†]Materials Science and Engineering, School for Engineering of Matter, Transport and Energy, Arizona State University, 501 E Tyler Mall, ECG 301, Tempe, Arizona 85287-6106, United States

[‡]Department of Chemistry and Biochemistry, Florida State University, Tallahassee, Florida 32306, United States

[§]Center for Interdisciplinary Magnetic Resonance, National High Magnetic Field Laboratory, 1800 East Paul Dirac Drive, Tallahassee, Florida 32310, United States

Supporting Information

ABSTRACT: Composite polymer solid electrolytes (CPEs) containing ceramic fillers embedded inside a polymer-salt matrix show great improvements in Li^+ ionic conductivity compared to the polymer electrolyte alone. Lithium lanthanum zirconate ($Li_7La_3Zr_2O_{12}$, LLZO) with a garnet-type crystal structure is a promising solid Li^+ conductor. We show that by incorporating only 5 wt % of the ceramic filler comprising undoped, cubic-phase LLZO nanowires prepared by electrospinning, the room temperature ionic conductivity of a polyacrylonitrile-$LiClO_4$-based composite is increased 3 orders of magnitude to 1.31×10^{-4} S/cm. Al-doped and Ta-doped LLZO nanowires are also synthesized and utilized as fillers, but the conductivity enhancement is similar as for the undoped LLZO nanowires. Solid-state nuclear magnetic resonance (NMR) studies show that LLZO NWs partially modify the PAN polymer matrix and create preferential pathways for Li^+ conduction through the modified polymer regions. CPEs with LLZO nanoparticles and Al_2O_3 nanowire fillers are also studied to elucidate the role of filler type (active vs passive), LLZO composition (undoped vs doped), and morphology (nanowire vs nanoparticle) on the CPE conductivity. It is demonstrated that both intrinsic Li^+ conductivity and nanowire morphology are needed for optimal performance when using 5 wt % of the ceramic filler in the CPE.

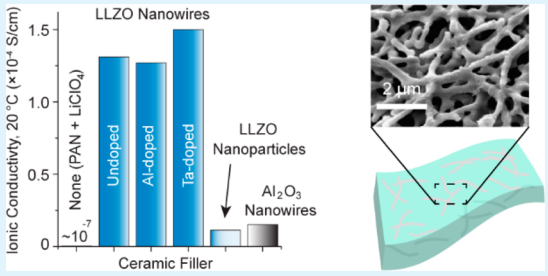

KEYWORDS: *composite polymer electrolyte, garnet-type solid electrolyte, nanowires, electrospinning, NMR, polyacrylonitrile*

INTRODUCTION

Recently, the development of solid Li^+ conducting electrolytes for all-solid-state batteries has attracted a great deal of research interest,[1] particularly since solid electrolytes have the potential to increase the safety characteristics of Li metal batteries,[2] mitigate the polysulfide dissolution issue in Li/S batteries,[3] and circumvent the organic electrolyte oxidation problem in Li/O_2 batteries.[4] Polymer-based electrolytes are attractive because they are not brittle and can more easily form interfaces to electrodes compared to inorganic electrolytes, but they also display poor mechanical properties and low ionic conductivities at room temperature.[5−7] The use of composite polymer electrolytes (CPEs) comprising a polymer electrolyte embedded with ceramic fillers has been an attractive strategy for enhancing the mechanical stability and ionic conductivity of the polymer.[5,6,8−11] The ceramic filler can increase the ionic transport of Li^+ in the CPE by several orders of magnitude, for example by decreasing the crystallinity of the conducting polymer and creating space charge regions that can enhance the Li^+ diffusion.[5,6,9,12,13]

While early studies investigated ceramic fillers comprising spherical particles of inert or "passive" components with no intrinsic Li^+ conductivity (*e.g.* Al_2O_3 and SiO_2),[9,14] recent advances in nanomaterials synthesis have enabled the development of novel CPEs containing fillers of "active" Li^+ conductors with nanowire (NW) morphologies. Electrospinning has emerged as a versatile and effective method to prepare oxide Li^+ conductors such as lithium lanthanum titanate ($Li_{3x}La_{2/3-x}TiO_3$, LLTO)[15,16] and lithium lanthanum zirconate ($Li_7La_3Zr_2O_{12}$, LLZO)[17,18] as NWs. So far, very promising results have been reported regarding the use of these materials as CPE fillers. LLTO NWs embedded into polyacrylonitrile (PAN) achieved 3 orders of magnitude improvement in room temperature Li^+ ionic conductivity compared to the polymer and Li^+ salt alone, but the mechanism was not thoroughly investigated.[16] A CPE prepared from a mat of Al-doped LLZO NWs infiltrated with poly(ethylene oxide) (PEO) was effective

Received: March 16, 2017
Accepted: June 9, 2017
Published: June 9, 2017

DOI: 10.1021/acsami.7b03806
ACS Appl. Mater. Interfaces 2017, 9, 21773−21780

for preventing Li dendrite formation under repeated lithium stripping/plating and also showed good flammability resistance.[18] Both studies attribute the long-range and continuous Li^+ diffusion pathways formed at the interfaces between the NWs and polymers as key to the improvements in conductivity. However, there are still many critical questions remaining, such as how the nature of the ceramic filler and its properties (*e.g.* morphology, composition) affect the total conductivity of the CPE and the mechanism of conductivity enhancement.

Our group's recent studies[17,19] on nanostructured LLZO have examined the role of particle and grain size on the phase stability of this garnet-type material. Nanostructured LLZO, either prepared by electrospinning, templating onto nanocellulose nanofibers, or ball-milling bulk powders, was observed to remain stable in the nonequilibrium cubic structure (c-LLZO) at room temperature without the use of extrinsic dopants. Calcining the c-LLZO induced grain growth and coalescence, which was correlated to the formation of the thermodynamically stable tetragonal phase (t-LLZO). As t-LLZO typically displays 2 orders of magnitude lower ionic conductivity than c-LLZO,[20] our findings point to a new way to access c-LLZO, namely through the use of nanostructures, which can subsequently be exploited as ceramic fillers for CPEs. This approach allows for the systematic study of different c-LLZO fillers (with and without dopants), in order to understand the critical parameters needed for CPEs with high ionic conductivity. The substitution of Al^{3+} on Li^+ sites[21−25] and Ta^{5+} on Zr^{4+} sites[22,26−29] can stabilize c-LLZO and create Li^+ vacancies, which could increase the number of hopping sites for Li^+.[20,27,29−31]

Herein we report the following: 1) the synthesis of undoped and doped (with Al or Ta) c-LLZO NWs using electrospinning from a dimethylformamide (DMF)-based precursor solution; 2) the evaluation of the aforementioned LLZO NWs as fillers in CPEs containing PAN and $LiClO_4$ using electrochemical methods, and 3) the determination of the Li^+ pathways through the CPEs using selective isotope labeling and solid-state Li nuclear magnetic resonance (NMR). We also evaluated CPEs containing c-LLZO nanoparticles (NPs) or Al_2O_3 NWs to understand the role of filler type (active vs passive), c-LLZO composition (undoped vs doped), and c-LLZO morphology (NW vs NP) on the total ionic conductivity of the CPE.

EXPERIMENTAL SECTION

More detailed descriptions about the experimental procedures can be found in the Supporting Information. Briefly, the LLZO nanowires were prepared using electrospinning from a precursor comprising zirconium propoxide, lithium nitrate, and lanthanum nitrate dissolved in a solution containing a mixture of acetic acid, *N*,*N*-dimethylformamide (DMF), and polyvinylypyrrolidone (PVP) as the polymer carrier. Aluminum nitrate or tantalum ethoxide was used to obtain doped samples with a nominal composition of $Li_{6.28}La_3Zr_2Al_{0.24}O_{12}$ and $Li_{6.5}La_3Zr_{1.5}Ta_{0.5}O_{12}$, respectively. The as-spun NWs were collected and calcined at 700 °C in air to remove the organic components and to crystallize the LLZO. The CPEs contained PAN and $LiClO_4$ at a weight ratio of 2:1 (*i.e.*, 33.3 wt % $LiClO_4$). EIS measurements were obtained from 5 MHz−1 Hz at various temperatures. Galvanostatic cycling measurements were carried out using a Li symmetric cell configuration in coin cells. ^6Li and ^7Li magic-angle-spinning NMR experiments were carried out on a Bruker Avance III-500 with Larmor frequencies of 73.6 and 194.4 MHz for ^6Li and ^7Li, respectively. A 2.5 mm Bruker HXY probe was used, and the samples were spun at 25 kHz. The $^{6,7}Li$ chemical shift was referenced to solid LiCl at 0 ppm.

RESULTS AND DISCUSSION

Our original method for preparing LLZO via electrospinning[17] used an aqueous solution containing LLZO sol−gel precursors mixed within a polymer solution, which resulted in the formation of nanowires after electrospinning, as shown in Figure 1a. Calcination of these nanowires at 700 °C for 3 h led to formation of c-LLZO characterized by interconnected "ligament"-like morphologies with dimensions of 100−200 nm (Figure 1b). In comparison, the c-LLZO NWs obtained using a DMF-based precursor solution showed improved fiberlike morphologies (Figure 1c) after calcination for 1 h

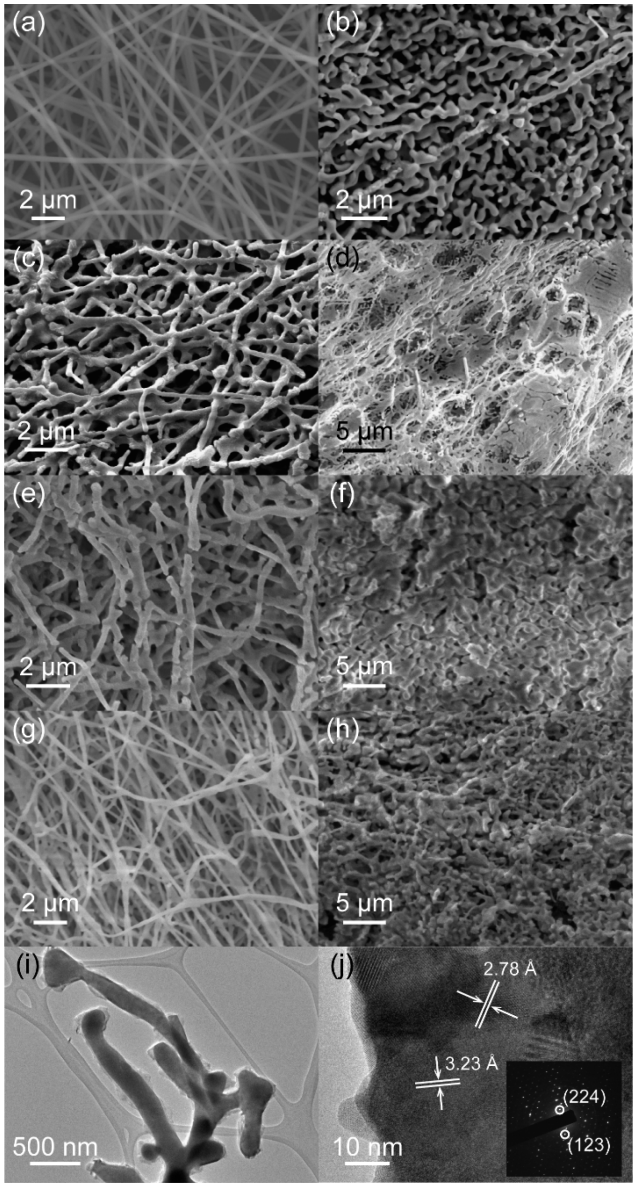

Figure 1. (a)-(h) are SEM images of electrospun nanowires. All calcinations were performed at 700 °C. (a) As-spun nanowires prior to calcination. (b) c-LLZO nanowires prepared using aqueous precursor and calcined for 3 h. (c)-(h): c-LLZO nanowires prepared using DMF-based precursor and calcined for (c), (e), (g) 1 h or (d), (f), (h) 3 h. (c)-(d): undoped LLZO, (e)-(f) Al-LLZO, (g)-(h) Ta-LLZO. (i) TEM image and (j) HRTEM image of undoped c-LLZO prepared from DMF-based precursor and calcined for 1 h. Inset is the corresponding SAED pattern.

DOI: 10.1021/acsami.7b03806
ACS Appl. Mater. Interfaces 2017, 9, 21773−21780

with an average diameter of 276 nm (Figure S1a). The Al-doped (Al-LLZO) (Figure 1e) and Ta-doped (Ta-LLZO) (Figure 1g) samples displayed similar morphologies as the undoped samples (Figure 1c), but the respective dopants were detectable using energy dispersive X-ray spectroscopy (EDS) (Figure S1b-c). Transmission electron microscopy (TEM) analysis revealed that the LLZO NWs were polycrystalline and became interconnected after calcination. Figure 1i shows the TEM image for undoped LLZO NWs calcined for 1 h, while Figure 1j is a high resolution TEM (HRTEM) image showing one region on a NW. The HRTEM image shows that each NW is made of multiple small grains with different shapes and sizes. The measured *d*-spacings were 3.23 and 2.78 Å, which corresponds to the interplanar distance of 3.24 Å for the (004) planes and 2.77 Å for the (233) planes, respectively, for c-LLZO.[20] The bottom-right inset is the selected-area electron diffraction (SAED) pattern of a few grains, with some major reflections labeled. As shown in the SEM and TEM images, if two nanowires were in contact with each other, they could merge and form a "junction" during calcination. Hence, the materials after calcination can be described as clusters or aggregates of multiple NWs connected together. In contrast, the c-LLZO NWs prepared from the aqueous precursor (Figure 1b) are characterized by ligaments with rounded ends and fewer connections with neighboring particles. Hence, the c-LLZO NWs prepared using the DMF-based precursors have more advantageous morphologies to serve as interconnected CPE fillers that can create continuous Li^+ diffusion pathways.

X-ray diffraction (XRD) analysis revealed that the undoped NW product crystallized in the cubic phase (Figure 2a). While the XRD pattern lacked the peak splitting on the major reflections (*e.g.* $2\theta \sim 16.6°$ and 30.5°)[23] that is characteristic of t-LLZO (Figure S2), a small degree of bifurcation (peak doublets) was present at some high angle reflections (Figure 2c), indicating the presence of some tetragonal distortion of the cubic lattice. Both Al-LLZO and Ta-LZZO samples also displayed XRD peak doublets as well (Figure 2c), suggesting that the dopants did not fully stabilize the c-LLZO structure. The rapid heat treatment (1 h calcination) likely resulted in a nonuniform distribution of dopants within the grains of the nanowires, leading to formation of c-LLZO (stabilized by dopants) and tetragonal distortion in undoped regions. This can also explain the presence of secondary phases in the two doped samples. $La_2Zr_2O_7$ was found in Al-LLZO and La_2O_3 in Ta-LLZO, which could be caused by incomplete reaction[32−34] or Li^+ loss due to volatilization during calcination,[32,35] with the former scenario being more likely since the heat treatment time was very short. Undoped samples subjected to 3 h calcination under the same conditions displayed particle coalescence and loss of the NW morphology (Figure 1d), along with more pronounced peak bifurcation in the XRD pattern (Figure 2c). This is consistent with our previous observations that longer heating can cause particle coalescence and increase the degree of tetragonal distortion and eventually lead to the formation of t-LLZO.[17]

For Al-LLZO and Ta-LLZO samples calcined for 3 h (Figure 1f and 1h, respectively), the NW morphology was destroyed by the heat treatment, but the t-LLZO peak doublets caused by tetragonal distortion disappeared (Figure 2c). These results show that the incorporation of dopants was indeed limited by the kinetics in this situation. Unlike our previous work, in which the NWs prepared from aqueous precursors required 3 h of calcination to completely crystallize into c-LZZO, the DMF-based nanowires required only 1 h to form the c-LLZO at the same temperature, even without requiring the dopants.

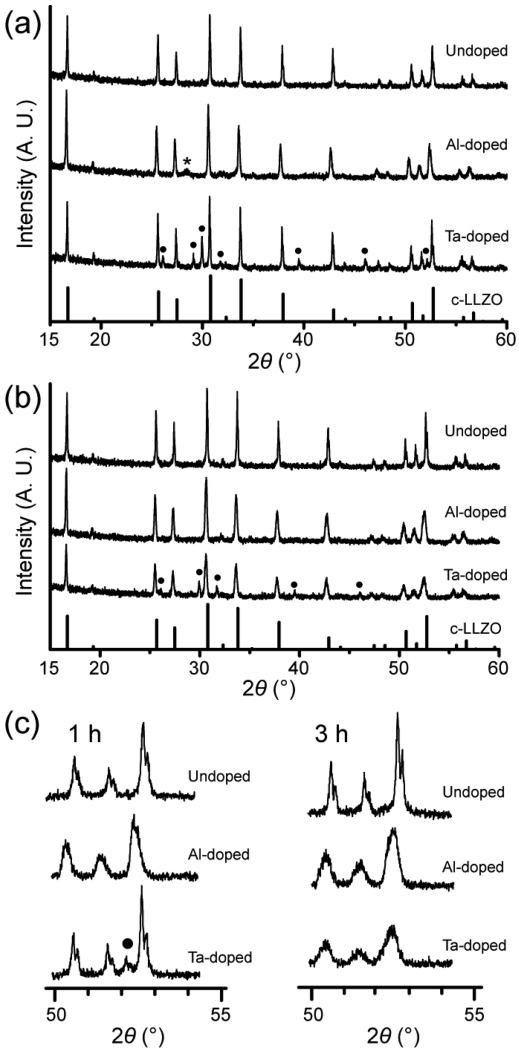

Figure 2. XRD patterns of LLZO nanowire samples after calcination for (a) 1 h and (b) 3 h, both at 700 °C. (c) Zoomed-in patterns at the region around $2\theta = 52°$. (*: $La_2Zr_2O_7$; ●: La_2O_3).

The SEM image in Figure 3a shows a top-down view of a CPE containing 5 wt % of undoped LLZO NWs prepared by stirring the NW powder into the polymer matrix solution (Supporting Information). The NWs were embedded within the polymer matrix, but the dispersion was not highly uniform, as some clusters/aggregates of NWs were observed. Due to the thickness of the CPE film, it is not easy to see the exact shape/morphology of the NWs, but for those that are closer to the top surface, the NW morphology is quite apparent (Figure S3a). To elucidate the effect of the CPE preparation (i.e., stirring) on the NW morphology, the polymer matrix solution was substituted with isopropyl alcohol, and the SEM results showed that the NWs could be found as individual particles and as clusters/aggregates after the stirring process (Figure S3b-e).

The CPEs were evaluated using EIS in the configuration illustrated in Figure 3b; the equivalent circuit used for data fitting is shown in Figure 3c, which was previously applied to CPEs containing ceramic fillers.[36] Here Q_c is a constant phase element for the bulk capacitance of the CPE, R_c is the overall resistance of the film, and Q_{el} is a constant phase element for the capacitances at the electrode interfaces. The total ionic

DOI: 10.1021/acsami.7b03806
ACS Appl. Mater. Interfaces 2017, 9, 21773−21780

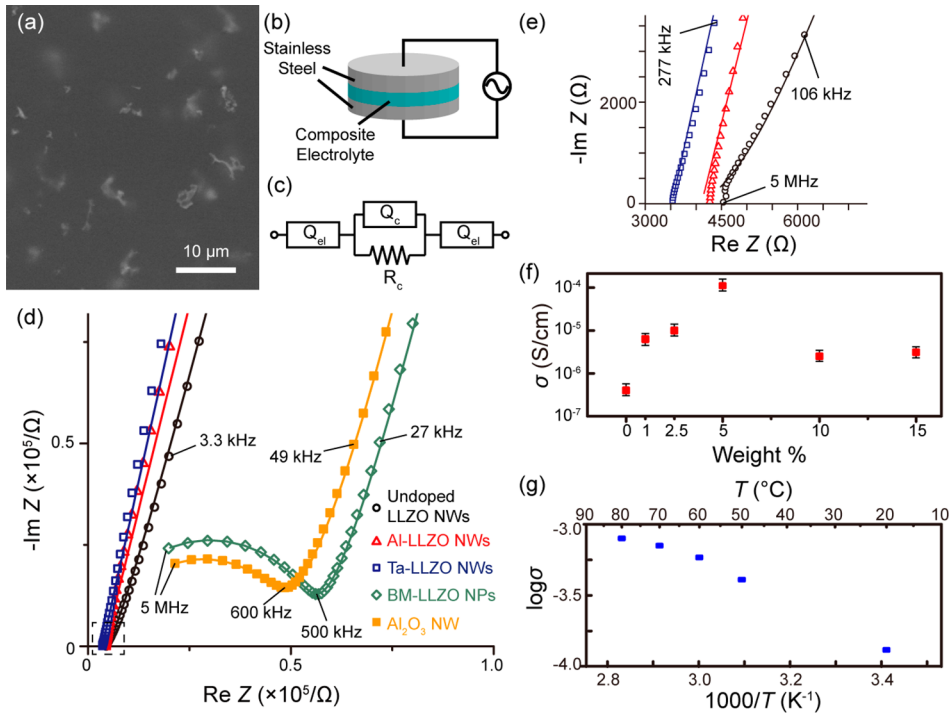

Figure 3. (a) SEM image (top-down view) of a CPE film. (b) Schematic of the EIS test setup. (c) Equivalent circuit used for EIS data fitting. (d) Representative Nyquist plots of CPEs embedded with 5 wt % of different filler materials, all tested at 20 °C. (e) Zoomed-in view of the region marked by dashed lines in (d). (f) Ionic conductivity comparison of CPEs embedded with different wt % of undoped LLZO NWs at 20 °C, with the conductivity of a blank sample for reference. Each point is the average of three measurements, and the error bars indicate the standard deviation. (g) Arrhenius plot of CPE with 5 wt % undoped LLZO NWs. Each point is the average of two measurements.

conductivity (σ) of the various representative CPEs obtained at 20 °C is displayed in Table 1, normalized by the thickness of each individual film. The associated Nyquist plots are shown in Figure 3d, with the high-frequency region shown in Figure 3e. As expected, all of the CPEs displayed higher conductivities than the blank sample containing only PAN and $LiClO_4$, which had an ionic conductivity ~10^{-7} S/cm and a Nyquist plot (Figure S4a) similar to previous reports.[10,16,37] Figure S4b shows the Nyquist plots of CPEs loaded with undoped LLZO NWs at different weight percentages. The peak conductivity of 1.31×10^{-4} S/cm was observed when using 5 wt % loading, but this decreased when the wt % of filler was increased further. This was likely due to an increase in aggregated NW clusters as the wt % increased, which was also observed in PAN-based CPEs containing LLTO NW fillers.[16] EIS measurements of the CPE containing 5 wt % of undoped LLZO nanowires were studied further at different temperatures (Figure S4c). The activation energy, E_a, was calculated to be 0.12 eV from the Arrhenius plot (Figure 3g), which is similar to the values reported for other PAN-based CPEs where Li^+ diffusion at the polymer/filler interface may be dominant.[10,16]

Table 1. Ionic Conductivity of Different Samples at 20 °C

ceramic type	wt % of filler	total ionic conductivity (S/cm)
none ($LiClO_4$ in PAN only)	0	4.06×10^{-7}
undoped LLZO NWs	1	6.17×10^{-6}
	2.5	1.00×10^{-5}
	5	1.31×10^{-4}
	10	2.52×10^{-6}
	15	3.10×10^{-6}
Al-doped LLZO NWs	5	1.27×10^{-4}
Ta-doped LLZO NWs	5	1.50×10^{-4}
BM-LLZO NPs	5	1.13×10^{-5}
Al_2O_3 NWs	5	1.52×10^{-5}

In order to investigate the effect of dopants in the LLZO on the overall ionic conductivity of the composite, CPEs loaded with 5 wt % Al- or Ta-LLZO NWs were prepared. The EIS results showed that the CPEs with doped LLZO NW fillers had similar ionic conductivities, ~10^{-4} S/cm, as the CPEs with undoped LLZO (Table 1), suggesting that the Li^+ conduction mechanism through the CPEs is dominated by a polymer/filler interface phenomenon that is independent of the LLZO filler composition. Undoped c-LLZO nanoparticles (average particle size ~25 nm, Figure S5) were prepared by ball-milling bulk t-LLZO (BM-LLZO NPs). The CPE with 5 wt % BM-LLZO NPs as fillers displayed a total ionic conductivity of 1.13×10^{-5} S/cm (Figure 3d), roughly an order of magnitude lower than the CPEs with LLZO NW fillers. This indicates that the NW morphology was important for the increased conductivity of the CPEs. Since the BM-LLZO NPs had much smaller diameters than the LLZO NWs, this suggests that the local continuous conduction pathways provided by the NWs are more important than the small particle diameters, which has previously been shown to play a large role in the plasticizing effect in polymers using spherical fillers.[9,38]

Since previous studies[16,39] have shown that the intrinsic ionic conductivity of the filler materials can also play an important role in the ionic conductivity of the CPE, 5 wt % Al_2O_3 NWs were used as passive fillers. The total ionic conductivity at room temperature was similar to the CPE with BM-LLZO NPs but still higher than the conductivity of the blank sample containing only PAN and $LiClO_4$. These results suggest that the ceramic

DOI: 10.1021/acsami.7b03806
ACS Appl. Mater. Interfaces 2017, 9, 21773−21780

fillers should be made of "active" Li^+ conductors with NW morphology in order to obtain CPEs with high ionic conductivity. However, since all of the LLZO NW samples displayed an ionic conductivity with similar order of magnitude, it appears that the presence of dopants is not crucial. Using the undoped c-LLZO NW as filler is advantageous because these materials had fewer impurities and better NW morphology than the doped samples.

To better understand the Li^+ local environment and transport mechanism in the LLZO-PAN CPEs, solid-state Li NMR was performed with selective ^{6}Li-isotope labeling and a ^{6}Li–^{7}Li isotope-replacement strategy. This method was established in a previous study in order to map out Li^+ pathways in CPEs comprising 50 wt % Al-doped LLZO particles in a PEO matrix; it was determined that there is preferential transport of Li^+ through the LLZO phase rather than the polymer phase or polymer-LLZO interface.[40] The method builds on the basis that ^{6}Li replaces ^{7}Li during Li^+ transport; by evaluating changes in the ^{6}Li amount in the CPE before and after electrochemical cycling, the Li^+ transport pathway can be determined. As shown in Figure 4a, the

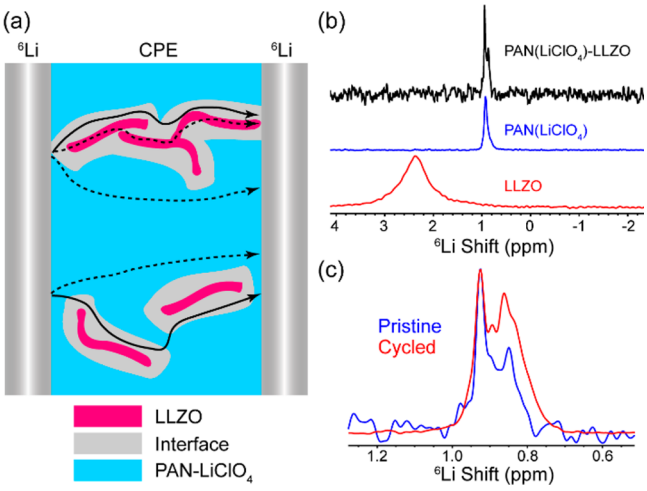

Figure 4. (a) Schematic showing possible Li^+ transport pathways in the CPE. (b) ^{6}Li NMR spectra of the CPE sample containing 5 wt % undoped LLZO NWs, a blank sample with only PAN and $LiClO_4$, and undoped LLZO NW powder. (c) ^{6}Li NMR spectra comparison between the as-made (pristine) and cycled CPEs containing 5 wt % undoped LLZO NWs. The cycled CPE had undergone 10 galvanostatic charge/discharge cycles in a symmetric ^{6}Li cell using 7.2 μA/cm^2.

possible Li^+ transport pathways in the CPE in this work are through the PAN polymer phase, through the LLZO NW phase, or through the interface region between the polymer and LLZO. In order to experimentally determine the actual Li^+ pathway in this CPE, it is necessary to first distinguish the Li ions in these three different local environments. Figure 4b shows the high-resolution ^{6}Li NMR spectra for the CPE containing 5 wt % undoped LLZO NWs, a blank film containing only PAN and $LiClO_4$, and the undoped LLZO NW powder. The ^{6}Li resonance in the undoped LLZO NWs was observed at 2.3 ppm, which is similar to what was observed in Al-doped LLZO in previous studies.[40] This resonance was not observed in the ^{6}Li NMR spectrum for the CPE, indicating that the amount of LLZO was too small. The ^{6}Li resonance of the $LiClO_4$ within the PAN in the blank film appeared at 0.90 ppm. In the NMR spectrum of the CPE, in addition to the 0.90 ppm peak, a new resonance was observed at 0.85 ppm. This resonance is attributed to $LiClO_4$ within the PAN with a local structural environment that is modified by the LLZO NW fillers. Quantification of the Li NMR spectrum of the CPE reveals that 37.4% of the Li resonates at 0.85 ppm and 62.6% of the Li at 0.90 ppm, which suggests that 37.4% of the PAN polymer matrix is modified by the LLZO NW filler.

To identify the preferred Li^+ diffusion pathway in the CPE, symmetric ^{6}Li foil/CPE/^{6}Li foil cells were assembled and tested galvanostatically (Figure S6). After 10 cycles, the ^{6}Li NMR spectrum was acquired. As shown in Figure 4c, the intensity of the resonance at 0.85 ppm increased after cycling, while the intensity of the resonance at 0.90 ppm did not change. This indicates that Li^+ prefers to travel through this LLZO-modified PAN phase rather than the unmodified PAN regions. This mechanism is different from what occurs in PEO-based CPEs containing 50 wt % Al-doped LLZO particles, wherein the Li^+ transport is preferred through an interconnected LLZO percolation network, despite the formation of a distinct local Li^+ environment at the LLZO/PEO interface that is detected using NMR.[40] For the films containing 5 wt % of LLZO NWs (corresponding to 2 vol %), there is insufficient LLZO to form a percolation network to enable Li^+ transport solely through the LLZO phase. However, these results show that for the PAN-based CPEs, very little LLZO is required to modify a significant fraction of the Li^+ local environment in the polymer phase and improve the ionic conductivity.

Unlike PEO-based CPEs, where ionic conductivity is increased by introduction of ceramic fillers acting as plasticizers to decrease the crystallinity of the polymer and enhance Li^+ transport through amorphous PEO regions,[9] previous studies demonstrated that introduction of ceramic fillers does not significantly change the crystallinity of PAN films containing Li^+ salts.[10,16] XRD of the blank sample and CPE with 5 wt % undoped LLZO NWs also confirmed that the PAN was amorphous in both cases (Figure S7). Instead, LLZO NW fillers could improve the ionic conductivity of the CPE by increasing the Li^+ dissociation from the ClO_4^- anion, which would increase the concentration of free Li^+ in the CPE.[37,41,42] This has been observed in CPEs using ceramic fillers with high dielectric constants and Lewis base surface groups with high affinity for the salt anion.[43,44] The dielectric constants (relative permittivities) of doped c-LLZO materials have been reported to be in the range of 40–60.[45,46] This is much higher than the dielectric constant of 9 for Al_2O_3,[47] indicating that LLZO can better promote ionic dissociation of the salt. Differences between the Lewis basicity of Al_2O_3 and LLZO may also explain the observed differences in conductivity for the CPEs containing either type of NW filler. Al_2O_3 is amphoteric and contains both surface Lewis acid centers (Al) and Lewis base centers (oxygen).[43] Although the acid–base properties of LLZO has, to our knowledge, not been thoroughly investigated yet, the negatively charged Li^+ vacancies created by Al[23,31,48] and Ta[49,50] doping should act as strong Lewis base centers. Li^+ vacancies may also play a role in the stabilization of the c-LLZO structure[23,49,51] in the undoped LLZO NW samples, although this needs to be further investigated. We also note that the ionic conductivities of our CPEs are of the same order of magnitude but roughly half of those reported by Liu et al.,[16] who observed a peak conductivity using 15 wt % LLTO NWs with an average diameter of 223 nm as ceramic fillers. Similar to LLZO, LLTO is also characterized by Li^+ vacancies.[52] Currently, it is not clear

DOI: 10.1021/acsami.7b03806
ACS Appl. Mater. Interfaces 2017, 9, 21773–21780

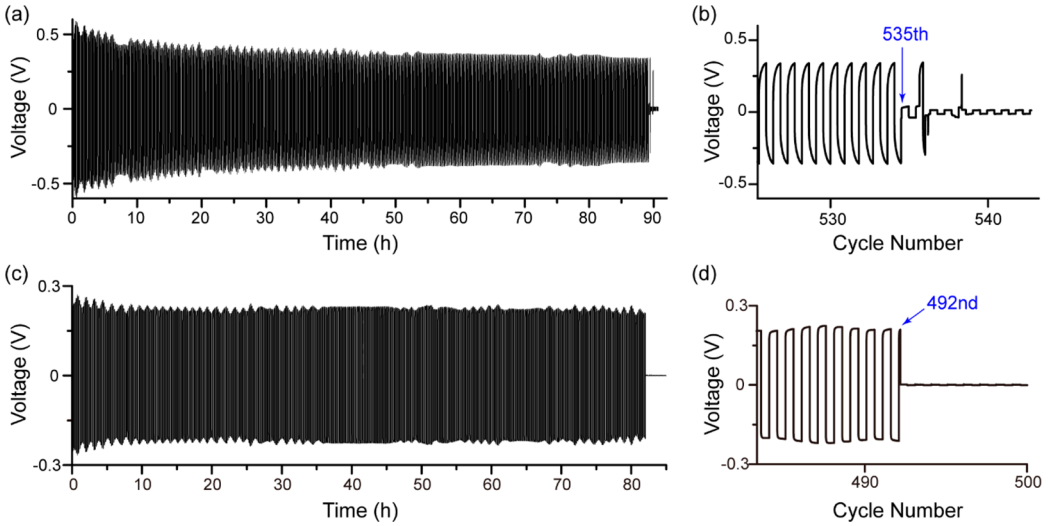

Figure 5. (a) Li symmetric cell galvanostatic cycling data of a CPE sample containing 5 wt % undoped LLZO NWs. (b) The tail region of (a), showing the sudden voltage drop. (c) Li symmetric cell galvanostatic cycling data of a blank sample. (d) The tail region of (c), showing the sudden voltage drop.

why only 5 wt % loading of LLZO NWs was needed to reach the peak CPE conductivity in our study, and why the peak value is lower than what was observed with the LLTO NWs. However, this could be due to differences in NW diameter and aggregation and differences in the intrinsic ionic conductivity of LLTO vs LLZO, in addition to the aforementioned dielectric and Lewis base properties of the materials. Also, since there was no elucidation of the conductivity-enhancing mechanism or Li^+ transport pathways in the study using LLTO NW fillers, there could be other potential causes that are still unknown.

The Li^+ transference number (t_{Li^+}) was determined using the method developed by Bruce et al.,[53] in which the CPE was sandwiched between two Li foils followed by application of a constant polarization voltage until the current reached a steady state. EIS was performed before and after the polarization, and t_{Li^+} = 0.3 at 20 °C was calculated from the experimental data obtained on the CPE with 5 wt % undoped LLZO NWs (Figure S8) using the method proposed by Lu et al.[54] (Supporting Information). To our knowledge, there have not been any reports on the t_{Li^+} for this type of system (PAN-$LiClO_4$-LLZO), but it is similar to the value of t_{Li^+} = 0.33 at 25 °C reported for a similar system (PAN-$LiClO_4$-Al_2O_3).[10] The electrochemical stability window was evaluated using cyclic voltammetry on a CPE film with 5 wt % undoped LLZO NWs (Figure S9). An anodic current in the first cycle was observed that could be due to side reactions or processes related to forming the interface with the Li metal electrodes; however, this feature was not present in subsequent cycles, and the expected Li stripping/plating behavior was observed.

Galvanostatic cycling was also performed to test the durability of the CPE sample containing 5 wt % undoped LLZO NWs (Figure 5a). The CPE film was sandwiched between two Li foils and tested at 20 °C, with a constant current density of 50 $\mu A/cm^2$ and changing the sign of the current every 300 s. It can be seen that there was an overall decrease in the cell voltage, which is similar to other studies.[18,55] At around the 535th cycle, a sudden voltage drop was observed (Figure 5b), which is characteristic of the penetration of the CPE by Li dendrites, leading to failure of the cell.[55,56] For comparison, a blank film containing no LLZO fillers was cycled under the same conditions, and the result is shown in Figure 5c. The overall cell voltage remained stable until it failed at the 492nd cycle (Figure 5d), which is about 92% of the lifetime of the CPE containing 5 wt % undoped LLZO NWs. It should be noted that the data presented in Figure 5b are the best cycling results obtained from our blank samples. All other blank samples either failed at very early stages (*e.g.* at the 221st cycle) or did not display stable cell voltages (Figure S10). These results imply that adding an appropriate amount of undoped LLZO NWs may have also reinforced the polymer matrix and made it mechanically stronger, similar to what has been observed in other nanocomposite polymer electrolytes,[9,16,18,40,57,58] which helped to resist the piercing of the CPE from growing Li dendrites. Further mechanical property testing in the future may help to shed light on this enhancement in cycling durability.

CONCLUSIONS

In summary, CPEs with LLZO NWs as ceramic fillers were fabricated and showed great improvement in the room-temperature ionic conductivity of a PAN-based polymer electrolyte to around 10^{-4} S/cm. The optimal mass loading for undoped LLZO NWs was determined to be 5 wt %. Doping of the LLZO did not have a pronounced influence on the ionic conductivity of the CPE, as films containing Al- and Ta-doped LLZO NWs displayed similar conductivity as those with the undoped LLZO NWs. Solid-state NMR measurements showed that the LLZO NWs partially altered the local environment of the PAN polymer matrix and that Li^+ diffusion occurred preferentially in the modified regions at the LLZO/polymer interface. We also demonstrated that both intrinsic ionic conductivity and NW morphology were required for the filler materials to achieve maximum effectiveness when used at 5 wt % in the CPE.

ASSOCIATED CONTENT

Supporting Information

The Supporting Information is available free of charge on the ACS Publications website at DOI: 10.1021/acsami.7b03806.

Experimental methods and characterization details; diameter distribution of c-LLZO nanowires; EDS spectra

DOI: 10.1021/acsami.7b03806
ACS Appl. Mater. Interfaces 2017, 9, 21773−21780

of doped c-LLZO nanowires; XRD comparison of t-LLZO and c-LLZO; SEM images of LLZO NWs in a CPE film and after stirring in an isopropyl alcohol solution; EIS data of blank CPE and CPEs with different weight percentages of undoped LLZO NWs; EIS data of CPE with 5 wt % undoped LLZO NWs at various temperatures; SEM and XRD of BM-LLZO; ^{6}Li foil symmetric galvanostatic cycling data of CPE with 5 wt % undoped LLZO NWs; XRD of blank CPE and CPE with 5 wt % undoped LLZO NWs; Li^+ transference number measurement data; electrochemical stability window data; Li symmetric galvanostatic cycling data of blank sample (PDF)

AUTHOR INFORMATION

Corresponding Author

*Phone: (480) 727-8614. E-mail: candace.chan@asu.edu.

ORCID

Candace K. Chan: 0000-0003-4329-4865

Author Contributions

The manuscript was written through contributions of all authors. T.Y. performed the materials synthesis/characterization and electrochemical measurements. Q.C. assisted with the CPE preparation. J.Z. performed the NMR measurements and ^{6}Li symmetric cell cycling. All authors have given approval to the final version of the manuscript.

Notes

The authors declare no competing financial interest.

ACKNOWLEDGMENTS

This work was supported by funding from NSF DMR-1553519. We gratefully acknowledge the use of facilities within the LeRoy Center for Solid State Science and Goldwater Environmental Laboratory at ASU. Y.-Y.H. acknowledges the support from NSF under Grant No. DMR-1508404. All solid-state NMR experiments were carried out at the National High Magnetic Field Laboratory (NHMFL) supported by NSF under contract DMR-1157490.

REFERENCES

(1) Chen, R.; Qu, W.; Guo, X.; Li, L.; Wu, F. The Pursuit of Solid-State Electrolytes for Lithium Batteries: From Comprehensive Insight to Emerging Horizons. *Mater. Horiz.* **2016**, *3* (6), 487−516.

(2) Ohta, S.; Kobayashi, T.; Seki, J.; Asaoka, T. Electrochemical Performance of an All-Solid-State Lithium Ion Battery with Garnet-Type Oxide Electrolyte. *J. Power Sources* **2012**, *202*, 332−335.

(3) McCloskey, B. D. Attainable Gravimetric and Volumetric Energy Density of Li-S and Li Ion Battery Cells with Solid Separator-Protected Li Metal Anodes. *J. Phys. Chem. Lett.* **2015**, *6* (22), 4581−4588.

(4) Girishkumar, G.; McCloskey, B.; Luntz, A. C.; Swanson, S.; Wilcke, W. Lithium-Air Battery: Promise and Challenges. *J. Phys. Chem. Lett.* **2010**, *1* (14), 2193−2203.

(5) Kumar, B.; Scanlon, L. G. Polymer-Ceramic Composite Electrolytes. *J. Power Sources* **1994**, *52* (2), 261−268.

(6) Wieczorek, W.; Florjanczyk, Z.; Stevens, J. R. Composite Polyether Based Solid Electrolytes. *Electrochim. Acta* **1995**, *40* (13−14), 2251−2258.

(7) Nairn, K.; Forsyth, M.; Every, H.; Greville, M.; MacFarlane, D. R. Polymer-Ceramic Ion-Conducting Composites. *Solid State Ionics* **1996**, *86−88*, 589−593.

(8) Przyluski, J.; Siekierski, M.; Wieczorek, W. Effective Medium Theory in Studies of Conductivity of Composite Polymeric Electrolytes. *Electrochim. Acta* **1995**, *40* (13−14), 2101−2108.

(9) Croce, F.; Appetecchi, G. B.; Persi, L.; Scrosati, B. Nanocomposite Polymer Electrolytes for Lithium Batteries. *Nature* **1998**, *394* (6692), 456−458.

(10) Chen-Yang, Y. W.; Chen, H. C.; Lin, F. J.; Chen, C. C. Polyacrylonitrile Electrolytes: 1. A Novel High-Conductivity Composite Polymer Electrolyte Based on PAN, $LiClO_4$ and α-Al_2O_3. *Solid State Ionics* **2002**, *150* (3−4), 327−335.

(11) Manuel Stephan, A.; Nahm, K. S. Review on Composite Polymer Electrolytes for Lithium Batteries. *Polymer* **2006**, *47* (16), 5952−5964.

(12) Jiang, S.; Wagner, J. B. A Theoretical Model for Composite electrolytes—I. Space Charge Layer as a Cause for Charge-Carrier Enhancement. *J. Phys. Chem. Solids* **1995**, *56* (8), 1101−1111.

(13) Croce, F.; Persi, L. L.; Scrosati, B.; Serraino-Fiory, F.; Plichta, E.; Hendrickson, M. A. Role of the Ceramic Fillers in Enhancing the Transport Properties of Composite Polymer Electrolytes. *Electrochim. Acta* **2001**, *46* (16), 2457−2461.

(14) Kim, J.-W.; Ji, K.-S.; Lee, J.-P.; Park, J.-W. Electrochemical Characteristics of Two Types of PEO-Based Composite Electrolyte with Functional SiO_2. *J. Power Sources* **2003**, *119−121*, 415−421.

(15) Yang, T.; Li, Y.; Chan, C. K. Enhanced Lithium Ion Conductivity in Lithium Lanthanum Titanate Solid Electrolyte Nanowires Prepared by Electrospinning. *J. Power Sources* **2015**, *287*, 164−169.

(16) Liu, W.; Liu, N.; Sun, J.; Hsu, P.-C.; Li, Y.; Lee, H.-W.; Cui, Y. Ionic Conductivity Enhancement of Polymer Electrolytes with Ceramic Nanowire Fillers. *Nano Lett.* **2015**, *15* (4), 2740−2745.

(17) Yang, T.; Gordon, Z. D.; Li, Y.; Chan, C. K. Nanostructured Garnet-Type Solid Electrolytes for Lithium Batteries: Electrospinning Synthesis of $Li_7La_3Zr_2O_{12}$ Nanowires and Particle Size-Dependent Phase Transformation. *J. Phys. Chem. C* **2015**, *119* (27), 14947−14953.

(18) Fu, K. K.; Gong, Y.; Dai, J.; Gong, A.; Han, X.; Yao, Y.; Wang, C.; Wang, Y.; Chen, Y.; Yan, C.; Li, Y.; Wachsman, E. D.; Hu, L. Flexible, Solid-State, Ion-Conducting Membrane with 3D Garnet Nanofiber Networks for Lithium Batteries. *Proc. Natl. Acad. Sci. U. S. A.* **2016**, *113* (26), 7094−7099.

(19) Gordon, Z. D.; Yang, T.; Gomes Morgado, G. B.; Chan, C. K. Preparation of Nano- and Microstructured Garnet $Li_7La_3Zr_2O_{12}$ Solid Electrolytes for Li-Ion Batteries via Cellulose Templating. *ACS Sustainable Chem. Eng.* **2016**, *4* (12), 6391−6398.

(20) Awaka, J.; Kijima, N.; Hayakawa, H.; Akimoto, J. Synthesis and Structure Analysis of Tetragonal $Li_7La_3Zr_2O_{12}$ with the Garnet-Related Type Structure. *J. Solid State Chem.* **2009**, *182* (8), 2046−2052.

(21) Geiger, C. A.; Alekseev, E.; Lazic, B.; Fisch, M.; Armbruster, T.; Langner, R.; Fechtelkord, M.; Kim, N.; Pettke, T.; Weppner, W. Crystal Chemistry and Stability of "$Li_7La_3Zr_2O_{12}$" garnet: A Fast Lithium-Ion Conductor. *Inorg. Chem.* **2011**, *50* (3), 1089−1097.

(22) Allen, J. L.; Wolfenstine, J.; Rangasamy, E.; Sakamoto, J. Effect of Substitution (Ta, Al, Ga) on the Conductivity of $Li_7La_3Zr_2O_{12}$. *J. Power Sources* **2012**, *206*, 315−319.

(23) Rangasamy, E.; Wolfenstine, J.; Sakamoto, J. The Role of Al and Li Concentration on the Formation of Cubic Garnet Solid Electrolyte of Nominal Composition $Li_7La_3Zr_2O_{12}$. *Solid State Ionics* **2012**, *206*, 28−32.

(24) Hubaud, A. A.; Schroeder, D. J.; Key, B.; Ingram, B. J.; Dogan, F.; Vaughey, J. T. Low Temperature Stabilization of Cubic $(Li_{7-x}Al_{x/3})La_3Zr_2O_{12}$: Role of Aluminum during Formation. *J. Mater. Chem. A* **2013**, *1* (31), 8813−8818.

(25) Matsui, M.; Takahashi, K.; Sakamoto, K.; Hirano, A.; Takeda, Y.; Yamamoto, O.; Imanishi, N. Phase Stability of a Garnet-Type Lithium Ion Conductor $Li_7La_3Zr_2O_{12}$. *Dalt. Trans.* **2014**, *43* (3), 1019−1024.

(26) Logéat, A.; Köhler, T.; Eisele, U.; Stiaszny, B.; Harzer, A.; Tovar, M.; Senyshyn, A.; Ehrenberg, H.; Kozinsky, B. From Order to Disorder: The Structure of Lithium-Conducting Garnets $Li_{7-x}La_3Ta_xZr_{2-x}O12$ (x = 0−2). *Solid State Ionics* **2012**, *206*, 33−38.

DOI: 10.1021/acsami.7b03806
ACS Appl. Mater. Interfaces 2017, 9, 21773−21780

(27) Adams, S.; Rao, R. P. Ion Transport and Phase Transition in $Li_{7-x}La_3(Zr_{2-x}M_x)O_{12}$ (M = Ta^{5+}, Nb^{5+}, X = 0, 0.25). *J. Mater. Chem.* **2012**, *22*, 1426−1434.
(28) Wang, Y.; Lai, W. High Ionic Conductivity Lithium Garnet Oxides of $Li_{7-x}La_3Zr_{2-x}Ta_xO_{12}$ Compositions. *Electrochem. Solid-State Lett.* **2012**, *15* (5), A68−A71.
(29) Miara, L. J.; Ong, S. P.; Mo, Y.; Richards, W. D.; Park, Y.; Lee, J.-M.; Lee, H. S.; Ceder, G. Effect of Rb and Ta Doping on the Ionic Conductivity and Stability of the Garnet $Li_{7+2x-y}(La_{3-x}Rb_x)$ $(Zr_{2-y}Ta_y)$-O_{12} ($0 \le X \le 0.375$, $0 \le Y \le 1$) Superionic Conductor: A First Principles Investigation. *Chem. Mater.* **2013**, *25*, 3048−3055.
(30) Buschmann, H.; Dölle, J.; Berendts, S.; Kuhn, A.; Bottke, P.; Wilkening, M.; Heitjans, P.; Senyshyn, A.; Ehrenberg, H.; Lotnyk, A.; Duppel, V.; Kienle, L.; Janek, J. Structure and Dynamics of the Fast Lithium Ion conductor "$Li_7La_3Zr_2O_{12}$. *Phys. Chem. Chem. Phys.* **2011**, *13* (43), 19378−19392.
(31) Zhang, Y.; Chen, F.; Tu, R.; Shen, Q.; Zhang, X.; Zhang, L. Effect of Lithium Ion Concentration on the Microstructure Evolution and Its Association with the Ionic Conductivity of Cubic Garnet-Type Nominal $Li_7Al_{0.25}La_3Zr_2O_{12}$ Solid Electrolytes. *Solid State Ionics* **2016**, *284*, 53−60.
(32) Kokal, I.; Somer, M.; Notten, P. H. L.; Hintzen, H. T. Sol−gel Synthesis and Lithium Ion Conductivity of $Li_7La_3Zr_2O_{12}$ with Garnet-Related Type Structure. *Solid State Ionics* **2011**, *185* (1), 42−46.
(33) Janani, N.; Ramakumar, S.; Dhivya, L.; Deviannapoorani, C.; Saranya, K.; Murugan, R. Synthesis of Cubic $Li_7La_3Zr_2O_{12}$ by Modified Sol-Gel Process. *Ionics* **2011**, *17*, 575−580.
(34) Sakamoto, J.; Rangasamy, E.; Kim, H.; Kim, Y.; Wolfenstine, J. Synthesis of Nano-Scale Fast Ion Conducting Cubic $Li_7La_3Zr_2O_{12}$. *Nanotechnology* **2013**, *24* (42), 424005.
(35) Murugan, R.; Thangadurai, V.; Weppner, W. Fast Lithium Ion Conduction in Garnet-Type $Li_7La_3Zr_2O_{12}$. *Angew. Chem., Int. Ed.* **2007**, *46* (41), 7778−7781.
(36) Qian, X.; Gu, N.; Cheng, Z.; Yang, X.; Wang, E. Impedance Study of $(PEO)_{10}LiClO_4$-Al_2O_3 Composite Polymer Electrolyte with Blocking Electrodes. *Electrochim. Acta* **2001**, *46* (12), 1829−1836.
(37) Yang, C. R.; Perng, J. T.; Wang, Y. Y.; Wan, C. C. Conductive Behaviour of Lithium Ions in Polyacrylonitrile. *J. Power Sources* **1996**, *62* (1), 89−93.
(38) Jayathilaka, P. A. R. D.; Dissanayake, M. A. K. L.; Albinsson, I.; Mellander, B.-E. Effect of Nano-Porous Al_2O_3 on Thermal, Dielectric and Transport Properties of the $(PEO)_9$LiTFSI Polymer Electrolyte System. *Electrochim. Acta* **2002**, *47* (20), 3257−3268.
(39) Wang, Y.-J.; Pan, Y.; Kim, D. Conductivity Studies on Ceramic $Li_{1.3}Al_{0.3}Ti_{1.7}(PO_4)_3$-Filled PEO-Based Solid Composite Polymer Electrolytes. *J. Power Sources* **2006**, *159* (1), 690−701.
(40) Zheng, J.; Tang, M.; Hu, Y.-Y. Lithium Ion Pathway within $Li_7La_3Zr_2O_{12}$ -Polyethylene Oxide Composite Electrolytes. *Angew. Chem.* **2016**, *128* (40), 12726−12730.
(41) Huang, B.; Wang, Z.; Li, G.; Huang, H.; Xue, R.; Chen, L.; Wang, F. Lithium Ion Conduction in Polymer Electrolytes Based on PAN. *Solid State Ionics* **1996**, *85* (1−4), 79−84.
(42) Huang, B.; Wang, Z.; Chen, L.; Xue, R.; Wang, F. The Mechanism of Lithium Ion Transport in Polyacrylonitrile-Based Polymer Electrolytes. *Solid State Ionics* **1996**, *91* (3−4), 279−284.
(43) Wieczorek, W.; Stevens, J. R.; Florjańczyk, Z. Composite Polyether Based Solid Electrolytes. The Lewis Acid-Base Approach. *Solid State Ionics* **1996**, *85* (1−4), 67−72.
(44) Golodnitsky, D.; Strauss, E.; Peled, E.; Greenbaum, S. Review—On Order and Disorder in Polymer Electrolytes. *J. Electrochem. Soc.* **2015**, *162* (14), A2551−A2566.
(45) Rettenwander, D.; Welzl, A.; Cheng, L.; Fleig, J.; Musso, M.; Suard, E.; Doeff, M. M.; Redhammer, G. J.; Amthauer, G. Synthesis, Crystal Chemistry, and Electrochemical Properties of $Li_{7-2x}La_3Zr_{2-x}Mo_xO_{12}$ (X = 0.1−0.4): Stabilization of the Cubic Garnet Polymorph via Substitution of Zr^{4+} by Mo^{6+}. *Inorg. Chem.* **2015**, *54* (21), 10440−10449.
(46) Rettenwander, D.; Redhammer, G.; Preishuber-Pflügl, F.; Cheng, L.; Miara, L.; Wagner, R.; Welzl, A.; Suard, E.; Doeff, M. M.; Wilkening, M.; Fleig, J.; Amthauer, G. Structural and Electrochemical Consequences of Al and Ga Cosubstitution in $Li_7La_3Zr_2O_{12}$ Solid Electrolytes. *Chem. Mater.* **2016**, *28* (7), 2384−2392.
(47) Robertson, J. High Dielectric Constant Oxides. *Eur. Phys. J.: Appl. Phys.* **2004**, *28* (3), 265−291.
(48) Miara, L. J.; Richards, W. D.; Wang, Y. E.; Ceder, G. First-Principles Studies on Cation Dopants and Electrolyte|cathode Interphases for Lithium Garnets. *Chem. Mater.* **2015**, *27* (11), 4040−4047.
(49) Thompson, T.; Wolfenstine, J.; Allen, J. L.; Johannes, M.; Huq, A.; David, I. N.; Sakamoto, J. Tetragonal vs. Cubic Phase Stability in Al-Free Ta Doped $Li_7La_3Zr_2O_{12}$ (LLZO). *J. Mater. Chem. A* **2014**, *2* (33), 13431−13436.
(50) Wang, Y.; Lai, W. Phase Transition in Lithium Garnet Oxide Ionic Conductors $Li_7La_3Zr_2O_{12}$: The Role of Ta Substitution and H_2O/CO_2 Exposure. *J. Power Sources* **2015**, *275*, 612−620.
(51) Bernstein, N.; Johannes, M. D.; Hoang, K. Origin of the Structural Phase Transition in $Li_7La_3Zr_2O_{12}$. *Phys. Rev. Lett.* **2012**, *109* (20), 205702.
(52) Stramare, S.; Thangadurai, V.; Weppner, W. Lithium Lanthanum Titanates: A Review. *Chem. Mater.* **2003**, *15* (21), 3974−3990.
(53) Bruce, P. G.; Evans, J.; Vincent, C. A. Conductivity and Transference Number Measurements on Polymer Electrolytes. *Solid State Ionics* **1988**, *28*−*30*, 918−922.
(54) Lu, Y.; Tikekar, M.; Mohanty, R.; Hendrickson, K.; Ma, L.; Archer, L. A. Stable Cycling of Lithium Metal Batteries Using High Transference Number Electrolytes. *Adv. Energy Mater.* **2015**, *5* (9), 1402073.
(55) Zhang, J.; Zhao, N.; Zhang, M.; Li, Y.; Chu, P. K.; Guo, X.; Di, Z.; Wang, X.; Li, H. Flexible and Ion-Conducting Membrane Electrolytes for Solid-State Lithium Batteries: Dispersion of Garnet Nanoparticles in Insulating Polyethylene Oxide. *Nano Energy* **2016**, *28*, 447−454.
(56) Pan, Q.; Smith, D. M.; Qi, H.; Wang, S.; Li, C. Y. Hybrid Electrolytes with Controlled Network Structures for Lithium Metal Batteries. *Adv. Mater.* **2015**, *27* (39), 5995−6001.
(57) Agrawal, R. C.; Pandey, G. P. Solid Polymer Electrolytes: Materials Designing and All-Solid-State Battery Applications: An Overview. *J. Phys. D: Appl. Phys.* **2008**, *41* (22), 223001.
(58) Agrawal, A.; Choudhury, S.; Archer, L. A. A Highly Conductive, Non-Flammable Polymer−nanoparticle Hybrid Electrolyte. *RSC Adv.* **2015**, *5* (27), 20800−20809.

DOI: 10.1021/acsami.7b03806
ACS Appl. Mater. Interfaces 2017, 9, 21773−21780